Meteoritics & Planetary Science 38, Nr 10, 1533–1546 (2003)
Abstract available online at http://meteoritics.org

Porosity and density of ordinary chondrites: Clues to the formation of friable and porous ordinary chondrites

Sarah L. WILKISON,[1*] Timothy J. McCOY,[2] Jane E. McCAMANT,[3]
Mark S. ROBINSON,[1, 4] and Daniel T. BRITT[5]

[1]Department of Geological Sciences, Northwestern University, 1850 Campus Drive, Evanston, Illinois 60208, USA
[2]Smithsonian Institution, Department of Mineral Sciences, Washington, D.C. 20560, USA
[3]Williams College, Williamstown, Massachusetts 01267, USA
[4]Center for Planetary Sciences, Northwestern University, Evanston, Illinois 60208, USA
[5]Department of Physics, University of Central Florida, Orlando, Florida 32816, USA
[*]Corresponding author. E-mail: sarah@earth.northwestern.edu

(Received 24 February 2003; revision accepted 26 August 2003)

Abstract–Densities and porosities of meteorites are physical properties that can be used to infer characteristics of asteroid interiors. We report density and porosity measurements of 42 pieces of 30 ordinary chondrites and provide a quantification of the errors of the gas pycnometer method used in this study. Based on our measurements, we find that no significant correlation exists between porosity and petrologic grade, chemical group, sample mass, bulk and grain density, or shock level. To investigate variations in porosity and density between pieces of a meteorite, we examined stones from two showers, Holbrook and Pultusk. Examination of nine samples of Holbrook suggests relative homogeneity in porosity and density between pieces of this shower. Measurements of three samples of Pultusk show homogeneity in bulk density, in contrast to Wilkison and Robinson (2000), a study that reported significant variations in bulk density between 11 samples of Pultusk. Finally, examination of two friable ordinary chondrites, Bjurböle and Allegan, reveal variability in friability and porosity among pieces of the same fall. We suggest that friable ordinary chondrites may have formed in a regolith or fault zone of an asteroid.

INTRODUCTION

Density and porosity are two intrinsic physical properties that describe the relationship between a mass and its unit volume. In the case of meteorites, these properties have been measured for more than a century (e.g., Merrill and Stokes 1900) and used to infer the mineralogy, mineral abundances, and pore spaces present in the meteorites and, by inference, in the asteroids from which they derive (e.g., Yomogida and Matsui 1983). Since 1990, flyby and orbiter missions (e.g., Galileo, NEAR) have directly measured the mass and volume of asteroids, revealing bulk densities that are significantly below those expected for analogue meteorites. This apparent mismatch between meteorite and asteroid densities has prompted several authors (i.e., Consolmagno and Britt 1998; Flynn et al. 1999; Wilkison and Robinson 2000; Wilkison et al. 2002; Britt et al. 2002) to revisit the issue of meteorite and asteroid physical properties using new techniques and a broader range of meteorites and meteorite types.

The density and porosity of a meteorite can be determined using several techniques including helium pycnometry and other displacement methods. The bulk density of an asteroid can be calculated from its mass and volume. The mass of an asteroid is determined by tracking spacecraft (e.g., Yeomans et al. 2000) or another asteroid (e.g., Belton et al. 1995); the volume can be determined from radiometry from the Infrared Astronomical Satellite (IRAS) Minor Planet Survey (Tedesco et al. 1992), occultation techniques (e.g., Millis and Dunham 1989), and spacecraft imaging or laser altimetry (e.g., Belton et al. 1995; Veverka et al. 1997; Zuber et al. 2000). Asteroid porosity can be inferred by comparing its measured density with that of a meteorite analogue. Microporosity is the inherent porosity of a meteorite that occurs on the same scale as the grain size and exists as small cracks and voids. Microporosity can be determined from the grain and bulk volumes of a sample. Grain volume is the volume of the mineral grains within the meteorite. Bulk volume is the total volume of the meteorite, including both the volume of the mineral grains and the volume occupied by pore spaces and cracks. The bulk density of a meteorite is its mass divided by its bulk volume; grain density is described as the mass of the meteorite divided by its grain volume.

© Meteoritical Society, 2003. Printed in USA.

Studies on ordinary chondrite meteorite porosities before 1998 used a variety of techniques and give little indication of the error in the measurement (see reviews in Consolmagno and Britt [1998] and Britt and Consolmagno [2003]). More recently, Consolmagno and Britt (1998) and Flynn et al. (1999) have used gas pycnometry and various bulk volume measurement techniques to determine the porosities for ~40 ordinary chondrites. Consolmagno and Britt (1998) measured the porosities of 42 pieces of 15 ordinary chondrites, ranging from 92 g to 1936 g, but most greater than 200 g. Flynn et al. (1999) measured the porosities of 23 pieces of 18 ordinary chondrites of mostly small (under 15 g mass) samples. Flynn et al. (1999) report the precision and accuracy of their measurement methods. Consolmagno and Britt (1998) report the precision of their porosity estimates but do not report the accuracy of the measurement techniques and how the accuracy affects their interpretations.

Mineralogical and chemical evidence point to an ordinary chondritic composition for the S-class asteroid 433 Eros (Trombka et al. 2000; Nittler et al. 2001; McFadden et al. 2001; McCoy et al. 2001; Evans et al. 2001). Wilkison et al. (2002) used the bulk densities and porosities (porosity range inferred from previous studies) of ordinary chondrite meteorites and the bulk density of the asteroid to infer the large-scale porosity (macroporosity) of Eros. Using this macroporosity estimate and other evidence, such as structural surface features (Prockter et al. 2002) and mass distribution models (Thomas et al. 2002a; Zuber et al. 2000), Wilkison et al. (2002) inferred that Eros is heavily fractured but still maintains internal strength. Because this conclusion was based on a range of porosities determined from measurements of a small number of ordinary chondrites, more porosities must be measured.

In this study, we report the porosities of 30 ordinary chondrite meteorites measured using gas pycnometry and modified Archimedian bead methods (Wilkison and Robinson 2000). In addition, a rigorous quantification of the systematic errors in our gas pycnometry method is provided. Potential controls of porosity, including petrologic type, mass, and shock level, are examined. The porosities of multiple pieces of two falls (Pultusk and Holbrook) were measured to determine the range of porosities and densities present within single ordinary chondrite falls. We also examine two particularly porous and friable ordinary chondrites (Allegan and Bjurböle) to further investigate whether these unweathered ordinary chondrites can be invoked as possible analogues to low-density asteroids, as suggested by Flynn et al. (1999).

METHODS

Meteorite samples were selected based on several criteria. Falls (not finds) were measured to minimize any potential porosity changes due to terrestrial weathering. Ordinary chondrites of moderate sizes (between 50 g and 1.2 kg) were selected. These sizes were chosen so that the samples were small enough to fit within the measurement chamber of the helium gas pycnometer and large enough to fill as much of that chamber as possible (see discussion below). We chose ordinary chondrites with a range of chemical groups (H, L, LL), petrologic types (4–6), and shock stages.

Bulk Volume

The bulk density of a meteorite is determined from the mass of the sample (measured on a Mettler digital balance) and the bulk volume, which is measured using a non-contaminating modified Archimedian method that uses small (250–425 μm size) glass beads to substitute for the liquid (Consolmagno and Britt 1998; Consolmagno et al. 1998). An in-depth discussion of the modified Archimedian method can be found in Consolmagno and Britt (1998) and Wilkison and Robinson (2000). This method of bulk volume measurement can have accuracy as high as 1% and a precision of 1.2% (Wilkison and Robinson 2000).

Grain Volume

A helium gas pycnometer was used to determine the grain volumes of the samples. Details of previous work with this specific apparatus are presented in Geddis (1994) and Consolmagno and Britt (1998). The pycnometer is composed of two cylindrical PVC chambers (approximately 1800 cm^3 and 2700 cm^3 internal volume) connected together by a valve (see Fig. 1). Chamber 1, the reservoir chamber, has an inlet valve that allows the input of helium gas. Chamber 2, the sample chamber, has a removable lid and an outlet valve that allows gas to be bled from the apparatus. Each chamber holds a pressure transducer that connects to a vibrating wire interface connected to a datalogger. The Geokon pressure transducers record the frequency of the vibrating wire within the transducer; the transducers have a measurement range between 0 to 1.72 bars (0 to 172368 N/m^2). Using the transducer calibration constants, we convert the output frequency into pressure. Measuring the pressure changes in the chambers before and after the gas is allowed to equilibrate between the two chambers allows us to calculate the volume of a sample. Research grade helium gas was chosen for this experiment because it easily diffuses into the pore spaces of the meteorite sample, it obeys the Ideal Gas Law at our operating conditions, and it does not contaminate the meteorite (Consolmagno and Britt 1998).

To measure grain volume using the pycnometer, the meteorite is placed into the sample chamber and the chamber lid is affixed to seal the system. The valve connecting the two chambers is closed. Using the inlet valve, helium is added until chamber 1 is pressurized to P_1 (2.0265 bars or 202650 N/m^2).

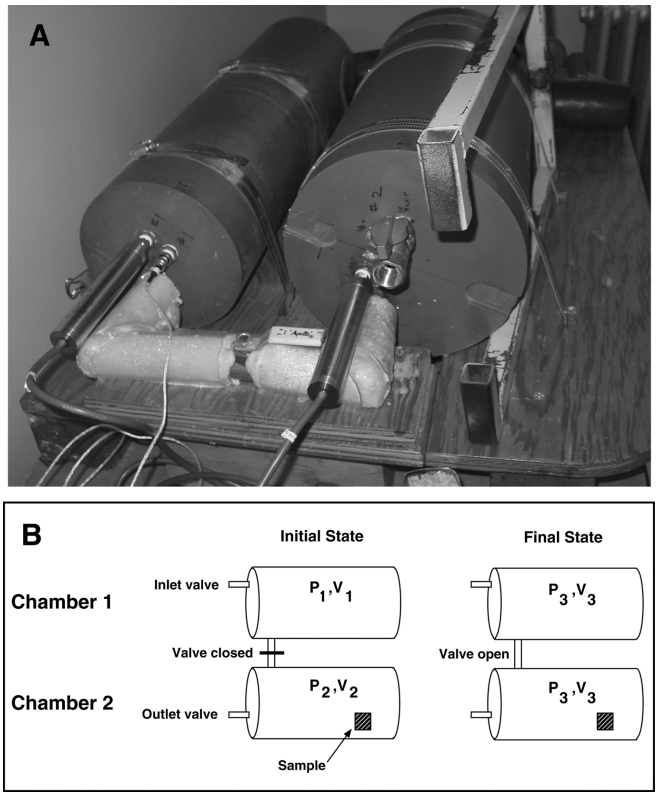


Fig. 1. a) Photograph of the helium gas pycnometer experimental setup. The larger chamber (V_2) is 22 cm in diameter, the smaller chamber (V_1) is 18 cm in diameter; b) cartoon illustrating the initial and final states of the experimental setup, as described in the text.

Chamber 2 is left at ambient pressure, P_2. We define this configuration as the "initial state" (see Fig. 1). In the initial state, chamber 1 (volume V_1) contains n_1 gas particles, and chamber 2 (volume V_2) contains n_2 gas particles. Applying the Ideal Gas Law to each chamber, we obtain the following equations:

$$P_1V_1 = n_1K_bT, \quad P_2V_2 = n_2K_bT \tag{1}$$

where *Kb* is the Boltzmann constant and *T* is the temperature in Kelvin (assumed to be the same in each chamber). In the initial state of the experiment, we measure the pressure within each chamber every 2 sec for about 7 min (total of 200 data points). The pressures are recorded via a datalogger interfaced with a laptop computer.

For the final state of the experiment, we open the valve between the chambers and allow the chambers to equilibrate for 30 sec. The final state has a pressure, P_3 (the average of the two pressure transducers), a combined volume, V_3 (=$V_1 + V_2$), and a total number of particles, n_3 (=$n_1 + n_2$). Assuming that no temperature change occurs during the expansion of the gas after the valve between the chambers is opened (based on a good approximation, the change in temperature is less than 0.1°C [Geddis 1994]), we may write:

$$P_1V_1 + P_2V_2 = P_3(V_1 + V_2). \tag{2}$$

Finally, we rearrange Equation 2 to solve for the ratio of the volumes of the empty space in the two chambers in terms of the output pressures:

$$V_2/V_1 = (P_3 - P_1)/(P_2 - P_3) \tag{3}$$

A new set of measurements (again, with 200 individual data points) is recorded after the chambers reach equilibrium. After the final state of the experiment has been recorded, the gas is leaked from the system. This process (of recording the pressures within the chambers for the initial and final states) is referred to as a trial. A total of five trials were recorded for each sample.

The grain volume cannot be determined explicitly from the ratio V_2/V_1 (the average ratio determined from the five trials). Instead, the grain volume is empirically determined by comparison to a calibration curve, which is itself derived from measurements of standards of known volume and porosity. We describe the derivation of this calibration curve below.

Billiard balls, known rock samples, and bricks were chosen as standards because they range from 0% to 67% porous, comparable to the potential range of ordinary chondrite porosities. The billiard balls are composed of phenolic resin and have a porosity of 0% (verified by an independent company specializing in commercial pycnometry, Core Labs). The diameters of the billiard balls were measured using a micrometer; the average volume of the balls is 96.990 ± 0.470 cm^3. Rock and brick samples of different porosities (ranging from 2–67%) were also measured for grain density and porosity by Core Labs. As a further check, a limestone with a porosity similar to that of a porous ordinary chondrite was sent to a second company (Micromeritics) for density and porosity measurement; the grain density results from the two companies are consistent (2.69 g/cm^3 and 2.70 g/cm^3).

Measurements of the billiard ball, rock, and brick samples were used to construct the calibration curve. A maximum of seven billiard balls can fit within the sample chamber; sets of 1–7 balls were measured with the pycnometer to create the calibration curve. The uncertainty in the actual volume of each billiard ball was taken to be zero in the calculation of the calibration curve. Sets of ball measurements were performed on each day that a sample was measured. The rock and brick samples of various porosities described above were also measured with the pycnometer and were included in the calibration curve using the company-determined grain densities as the "known" grain densities. In total, over 115 sets of measurements were used to construct the calibration curve.

We determined the calibration curve (Fig. 2) by fitting a polynomial to the standards' measurements (i.e., the known volumes and ratios) and minimizing the χ^2 (chi square) statistic. The relation between the ratio of the volumes of the two chambers and the volume of the sample is nearly linear; higher-order polynomials, however, did not improve the chi square over the linear fit. The final relation between the ratio

V_2/V_1 (obtained from Equation 3) and V_{grain} (the grain volume) is:

$$V_2/V_1 = (1.4803 \pm 0.0004736) + (-0.0054507 \pm 1.4037 \times 10^{-6})\,(V_{grain}) \quad (4)$$

The reduced chi square is 1.2, indicating that we have calculated reasonable errors for the fit parameters of the calibration equation. The error on the fit parameters represents the error expected from the pressure transducers, the statistical error of the five trials measured, and other systematic errors such as fluctuations in environmental conditions.

To determine if the apparatus could accurately measure the absolute pressure within the chambers, the ambient pressure determined by the pycnometer was compared to the ambient pressure measured by a portable barometer. Based on this comparison, we conclude that a shift in the transducers' factory calibration constants has occurred that does not allow the apparatus to accurately (at least at the level of uncertainty we are interested in) determine absolute pressure. However, further tests show that the transducers can accurately (within quoted error of the factory calibration, $\pm 5.17 \times 10^{-4}$ bars [or 51.71 N/m^2]) detect relative differences in pressure between the two chambers. Therefore, to reduce systematic errors introduced by trying to account for the shift in the constants of the transducers, we modify Equation 3:

$$V_2/V_1 = (P_{3(1)} - P_1)/(P_2 - P_{3(2)}) \quad (5)$$

where in this case, $P_{3(1)}$ is the pressure measured in chamber 1, and $P_{3(2)}$ is the pressure in chamber 2 after the valve has been opened and mixing between chambers has occurred.

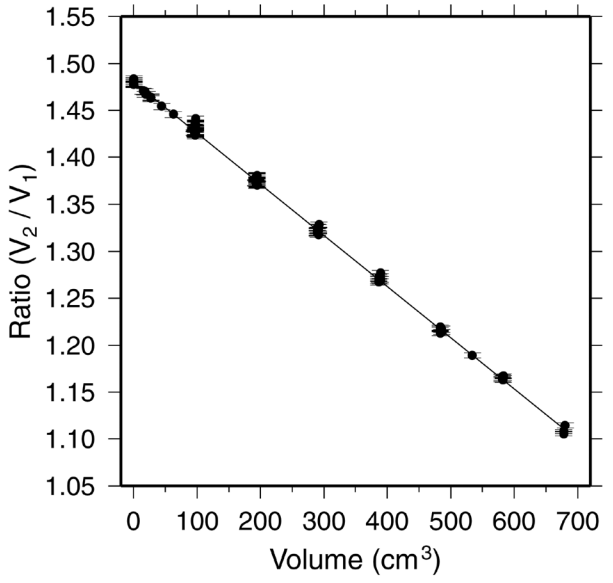


Fig. 2. The ratio (V_2/V_1) determined from the gas pycnometer is plotted versus the volume of the billiard balls. The line that best fits the data (Equation 4) is also plotted. The correlation coefficient (r) is 0.99, indicating a strong linear correlation. The grain volume of a sample is empirically determined by comparison to this calibration curve.

Many environmental conditions can potentially affect the pressure transducers; however, not all of them may be applicable to our experiment. Our equipment was located in a climate-controlled room. We experienced slight temperature and barometric changes, changes in personnel (S. Wilkison, J. McCamant), nearby construction activity, and seasonal changes.

One source of error we evaluated was fluctuations in temperature and humidity. The calibration curve is derived from measurements of standards throughout the experiment, thus, it incorporates daily and seasonal variations in temperature and humidity. We noticed a slight increase in the ratio (V_2/V_1) over a large range of temperature and relative humidity (22.7–26.6°C; 20–56%). However, within normal operating conditions (22.7–25.0°C; 30–50%), the ratio is essentially invariant (±0.012 about the central value, which is ~3 times the ±0.004 produced by the error in the pressure transducers alone). This spread in the ratio can be understood as the random distribution of the data within the uncertainty of the pressure transducers.

Porosity of a sample is determined from the grain and bulk volumes determined using the methods described above and is expressed as:

$$\% \text{ Porosity} = [1 - (V_{grain} / V_{bulk})] \times 100 \quad (6)$$

Based on our analysis of the pycnometer, we conclude that the error on the grain volume dominates the uncertainty of the porosity estimate and that smaller sized samples are more affected by the grain volume error (Fig. 3). For smaller sized samples, we are, at the least, providing a reasonable porosity range, even if we are unable to pinpoint an absolute porosity. In general, the pycnometer gives accurate measurements of the grain volume to ~±6 cm^3. The fractional error in the grain

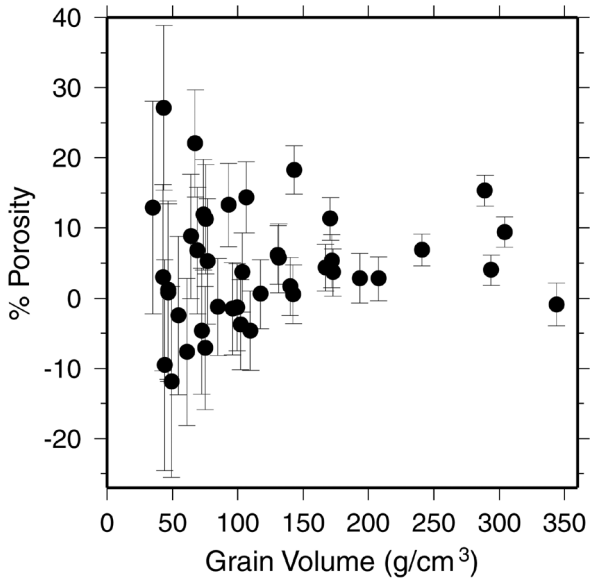


Fig. 3. Plot of percent porosity versus grain volume. Smaller sized samples are more affected by the error in grain volume (~±6 cm^3).

volume of smaller sized samples is larger than that of larger sized samples. For example, a sample with a grain volume of 35 cm^3 ± 6 cm^3 and a porosity of 12%, results in a porosity estimate of 0–28%, while a sample with a grain volume of 300 cm^3 ± 6 cm^3 and a porosity of 12% returns a porosity range of 10–14%.

Implications for Previous Studies with This Pycnometer

Quantifying the error in the grain volume measurement of this pycnometer has important implications for the interpretation of previously published data (e.g., Consolmagno and Britt 1998). The error in grain volume reported in Consolmagno and Britt (1998) is simply the formal errors of the repeatability (precision) of the grain volume measurement based on the five measurement trials taken of each sample. The porosity error listed in Consolmagno and Britt (1998) is a formal error calculated from both the measurement error of the bulk volume and the measurement error of the grain volume; these errors do not include an accuracy estimate. The reported error in this study includes both repeatability (based on the five trials taken of each sample) and accuracy (based on the manufactures' quote of error on the calibration of the pressure transducers and the errors on the parameters that compose the calibration curve). Differences between the first setup site (Arizona) (Geddis 1994), the second site (Italy) (Consolmagno and Britt 1998), and our location (Illinois) include elevation and climate changes. If the pycnometer was similarly calibrated at the second site (Italy) as it was at the site for our study (Illinois), we can reasonably believe that the ±6.0 cm^3 error in grain volume could be applied to the previous measurements. The grain volume error puts realistic bounds on the porosity range for a given sample, increasing the uncertainty in the porosity of samples previously measured by this pycnometer. However, most of the ordinary chondrite meteorites measured by Consolmagno and Britt (1998) had total masses larger than 200 g and, thus, would not be as affected by the grain volume error. This result indicates that the majority of the ordinary chondrite grain volume measurements from Consolmagno and Britt (1998) are reliable.

RESULTS

We measured the grain densities, bulk densities, and porosities of 42 pieces of 30 ordinary chondrites (Table 1); the uncertainty is at the 1σ level. Some meteorites were too small to be measured meaningfully for grain volume in the pycnometer but were measured for bulk density (also listed in Table 1). The mean value of sample porosities range from –12 to 27%, with 95% of samples below 20% (Table 1). Negative porosities are consistent with zero after taking into account the error in the measurement. Because smaller samples have greater errors associated with them, we calculate a weighted average that takes the uncertainties in the measurements into account. The weight is defined as the reciprocal square of the corresponding uncertainty of the value. The weighted averages of porosity of the LL, L, and H groups are listed in Table 2. The weighted average porosity of all ordinary chondrite samples (n = 42) is 6.4% ± 0.7%. The median porosity value of the data set (n = 42) is 3.7%. The (non-weighted) average of only those porosity measurements with less than ±5% porosity error (n = 18) is 6.2%. The weighted average grain density (n = 42) is 3.51 g/cm^3, with a range between 3.00 ± 0.29 g/cm^3 and 4.57 ± 0.44 g/cm^3.

DISCUSSION

Controls on Porosity

Different physical and chemical processes may affect the porosity of a meteorite at various stages of its history: accretion of materials, burial and lithification, thermal metamorphism, aqueous alteration, brecciation, and shock. We address the influence of several of these processes, such as thermal metamorphism (through the examination of petrologic grade) and shock. To investigate the key controls on our observed range of porosity (–12 to 27%), we compare our porosity results to ordinary chondrite petrologic grade, chemical group, mass, bulk and grain density, brecciation, and shock.

Petrologic grade represents the amount of heating the ordinary chondrite has undergone, possibly representing the meteorite's depth of burial within the parent asteroid (Herndon and Herndon 1977; Minster and Allegre 1979; Pellas and Storzer 1981; Miyamoto and Fujii 1980; Miyamoto et al. 1981; Scott and Rajan 1981; Taylor et al. 1982; Grimm 1985; McCoy et al. 1990). Consistent with previous studies (Consolmagno and Britt 1998; Flynn et al. 1999), we find no correlation between porosity and petrologic grade (Fig. 4). Thus, the heating process by which the meteorite was metamorphosed (i.e., depth of burial) has no observable effect on the porosity of the material.

Equilibrated ordinary chondrites are classified into three chemical groups (H, L, LL) based on composition and mineralogical parameters such as mol% Fa in olivine, mol% Fs in orthopyroxene, and total Fe (cf., Gomes and Keil 1980). Our data indicate no correlation between porosity and ordinary chondrite chemical group (Fig. 5).

Sample masses range from 124.1 g to 1191.8 g in this study. As discussed above, smaller sized samples are more affected by the grain volume error associated with the pycnometer setup. We considered that there might be some observable systematic change in porosity as a function of sample mass due to the grain volume measurement error. We find no correlation between porosity and sample mass (Fig. 6). Note that this figure also illustrates the systematic error associated with the grain volume measurement; samples with less mass have higher porosity errors than samples with more mass.

Table 1. Density and porosity measurements of ordinary chondrite meteorites.

Meteorite	Sample no.[a]	Type	Shock level	Mass (g)	Grain vol. (cm^3)	Grain dns. (g/cm^3)	Bulk vol. (cm^3)	Bulk dns. (g/cm^3)	Porosity (%)
Alfianello	FMNH ME 334	L6	S5[b]	279.70	73.8 ± 6.5	3.79 ± 0.34	83.7 ± 1.1	3.34 ± 0.04	11.9 ± 7.9
Allegan	FMNH ME 1430	H5	S1[c]	124.10	35.1 ± 6.1	3.54 ± 0.61	40.3 ± 0.5	3.08 ± 0.04	12.9 ± 15.1
	FMNH ME 1432	H5	S1[c]	186.05	43.3 ± 6.9	4.29 ± 0.69	59.4 ± 0.7	3.13 ± 0.04	27.1 ± 11.7
Barbotan	FMNH ME 1844	H5	S3 (sv)[d]	307.44	67.3 ± 6.6	4.57 ± 0.44	86.4 ± 1.1	3.56 ± 0.05	22.0 ± 7.7
Beaver Creek	FMNH ME 1393	H4	S2	1102.10	289.0 ± 6.7	3.81 ± 0.09	341.3 ± 4.0	3.23 ± 0.04	15.3 ± 2.2
Bjurböle	NMNH 695	L4	S1[b]	142.01	46.8 ± 6.0	3.03 ± 0.39	47.2 ± 0.7	3.01 ± 0.04	0.8 ± 12.7
Blanket	FMNH ME 1965	L6	–	1191.80	343.6 ± 9.4	3.47 ± 0.09	340.5 ± 4.5	3.50 ± 0.05	–0.9 ± 3.1
Cabezo de Mayo[e]	FMNH ME 1514	L6	–	102.20	–	–	30.4 ± 0.4	3.36 ± 0.04	–
Dhurmsala	FMNH ME 1346	LL6	S3[b]	278.05	76.6 ± 7.2	3.63 ± 0.34	80.8 ± 1.1	3.44 ± 0.05	5.2 ± 8.9
	FMNH ME 1347	LL6	S3[b]	985.40	293.8 ± 5.2	3.35 ± 0.06	306.0 ± 4.2	3.22 ± 0.04	4.0 ± 2.1
Ergheo	FMNH ME 1769	L5	S3 (sv)	383.81	106.4 ± 6.0	3.61 ± 0.21	124.2 ± 2.0	3.09 ± 0.05	14.4 ± 5.1
Fisher	FMNH ME 1341	L6	S5[f]	276.55	84.9 ± 5.7	3.26 ± 0.22	83.8 ± 1.0	3.30 ± 0.04	–1.3 ± 6.9
Forest City[e]	FMNH ME 1810	H5	S2[b]	491.30	142.4 ± 5.6	3.45 ± 0.13	143.2 ± 2.2	3.43 ± 0.05	0.6 ± 4.2
Hamlet	FMNH ME 2574	LL4	S3[b]	560.69	143.2 ± 5.8	3.92 ± 0.16	175.2 ± 2.1	3.20 ± 0.04	18.3 ± 3.4
Holbrook	FMNH ME 2022	L6	S2	461.86	140.2 ± 5.7	3.30 ± 0.13	142.5 ± 1.5	3.24 ± 0.03	1.7 ± 4.1
	FMNH ME 2023	L6	S2	316.65	99.3 ± 5.9	3.19 ± 0.19	98.0 ± 1.3	3.23 ± 0.04	–1.3 ± 6.2
	FMNH ME 2027	L6	S2	377.72	117.4 ± 5.6	3.22 ± 0.15	118.0 ± 1.4	3.20 ± 0.04	0.6 ± 4.9
	FMNH ME 2028	L6	S2	573.31	172.6 ± 5.7	3.32 ± 0.11	179.2 ± 2.1	3.20 ± 0.04	3.7 ± 3.4
	FMNH ME 2029	L6	S2	557.50	167.2 ± 5.5	3.33 ± 0.11	174.8 ± 1.8	3.19 ± 0.03	4.3 ± 3.3
	NMNH 2272	L6	S2	157.37	46.7 ± 6.0	3.37 ± 0.43	47.3 ± 0.7	3.33 ± 0.05	1.1 ± 12.7
	NMNH 437	L6	S2	448.10	130.6 ± 5.6	3.43 ± 0.15	139.2 ± 1.6	3.22 ± 0.04	6.2 ± 4.2
	NMNH 569–138	L6	S2	138.09	44.1 ± 6.0	3.13 ± 0.42	40.3 ± 0.9	3.43 ± 0.08	–9.5 ± 15.0
	NMNH 569–234	L6	S2	234.32	75.1 ± 6.0	3.12 ± 0.25	70.2 ± 1.1	3.34 ± 0.05	–7.1 ± 8.7
Jelica[e]	FMNH ME 511	LL6	–	64.17	–	–	19.4 ± 0.2	3.30 ± 0.04	–
Kesen	FMNH ME 258	H4	S3[b]	1188.00	304.0 ± 5.6	3.91 ± 0.07	335.6 ± 5.1	3.54 ± 0.05	9.4 ± 2.2
Knyahinya[e]	FMNH ME 286	L5	S3	239.52	72.3 ± 6.1	3.31 ± 0.28	69.0 ± 0.9	3.47 ± 0.05	–4.7 ± 8.9
Leighton[e]	FMNH ME 768	H5	–	302.00	75.5 ± 6.6	3.99 ± 0.35	85.1 ± 0.9	3.55 ± 0.04	11.2 ± 7.8
Limerick	FMNH ME 1795	H5	S3[g]	51.20	–	–	14.8 ± 0.3	3.46 ± 0.06	–
Lissa	FMNH ME 1410	L6	–	150.09	42.8 ± 5.8	3.50 ± 0.48	44.1 ± 0.6	3.40 ± 0.05	2.9 ± 13.3
Lixna	FMNH ME 1764	H4	–	61.59	–	–	17.2 ± 0.2	3.58 ± 0.05	–
Menow	FMNH ME 1388	H4	S1	585.61	170.8 ± 5.6	3.43 ± 0.11	192.6 ± 2.0	3.04 ± 0.03	11.3 ± 3.0
Mocs	FMNH ME 1445	L6	S3 (sv)	840.40	240.8 ± 5.3	3.49 ± 0.08	258.6 ± 2.7	3.25 ± 0.03	6.9 ± 2.3
Monze	FMNH ME 2441	L6	–	153.00	–	–	43.5 ± 0.5	3.52 ± 0.04	–
Nerft	FMNH ME 1637	L6	–	61.37	–	–	17.5 ± 0.3	3.51 ± 0.05	–
New Concord	FMNH ME 1825	L6	S3	650.30	193.2 ± 5.8	3.37 ± 0.10	198.9 ± 4.2	3.27 ± 0.07	2.8 ± 3.5
Nuevo Mercurio	FMNH ME 2818	H5	–	53.26	–	–	16.8 ± 0.2	3.17 ± 0.04	–
Ochansk[e]	FMNH ME 1441	H4	S3[b]	741.00	207.6 ± 5.3	3.57 ± 0.09	213.5 ± 4.3	3.47 ± 0.07	2.8 ± 3.1
Olivenza	FMNH ME 2095	LL5	S3[b]	179.70	54.6 ± 6.0	3.29 ± 0.36	53.3 ± 0.7	3.37 ± 0.05	–2.5 ± 11.3
Pultusk[e]	FMNH ME 1582	H5	S3[b]	354.12	102.1 ± 5.9	3.47 ± 0.20	98.4 ± 2.2	3.60 ± 0.08	–3.8 ± 6.4
	FMNH ME 1583	H5	S3[b]	370.98	109.7 ± 5.8	3.38 ± 0.18	104.8 ± 1.2	3.54 ± 0.04	–4.6 ± 5.7
	FMNH ME 1588	H5	S3[b]	645.70	171.7 ± 6.6	3.76 ± 0.14	181.4 ± 2.1	3.56 ± 0.04	5.3 ± 3.8
Segowlie	FMNH ME 1865	L6	S1	166.32	49.4 ± 5.9	3.37 ± 0.40	44.1 ± 0.9	3.77 ± 0.08	–11.9 ± 13.6
Sevrukovo	FMNH ME 1602	L5	–	130.78	–	–	37.0 ± 0.7	3.53 ± 0.07	–
Sindhri	FMNH ME 573	H5	S2	351.24	103.5 ± 5.9	3.40 ± 0.20	107.4 ± 1.3	3.27 ± 0.04	3.7 ± 5.6
Soko-Banja[e]	FMNH ME 1373	LL4	S2	241.73	69.1 ± 6.6	3.50 ± 0.33	74.2 ± 1.4	3.26 ± 0.06	6.8 ± 9.0
Ställdalen[e]	FMNH ME 1658	H5	S4 (sv)	341.68	95.8 ± 6.1	3.57 ± 0.22	94.4 ± 1.2	3.62 ± 0.05	–1.5 ± 6.6
Saint-Séverin	FMNH ME 2664	LL6	–	207.00	–	–	61.1 ± 0.8	3.39 ± 0.05	–
Tsarev	FMNH ME 3099	L5	–	82.10	–	–	24.5 ± 0.4	3.35 ± 0.06	–
Tuxtuac	FMNH ME 2850	LL5	S1	339.78	93.0 ± 6.3	3.65 ± 0.25	107.2 ± 1.1	3.17 ± 0.03	13.3 ± 5.9
Vouillé	FMNH ME 1663	L6	S3	453.99	131.3 ± 5.7	3.46 ± 0.15	139.3 ± 4.1	3.26 ± 0.10	5.7 ± 4.9
Weston	FMNH ME 2751	H4	S1	183.46	61.2 ± 5.8	3.00 ± 0.29	56.8 ± 1.2	3.23 ± 0.07	–7.7 ± 10.5
Zavid[e]	FMNH ME 1861	L6	S3	248.39	64.2 ± 6.1	3.87 ± 0.37	70.4 ± 1.2	3.53 ± 0.06	8.8 ± 8.8

[a]FMNH = samples from the Field Museum of Natural History; NMNH = samples from the National Museum of Natural History.
[b]Shock value from Stöffler et al. (1991).
[c]Shock value from Rubin (1992).
[d](sv) indicates opaque shock veins.
[e]Classified as brecciated (Grady 2000).
[f]Shock value from Bennett and McSween (1996).
[g]Shock value from Rubin (1994).

Table 2. Average porosity and density values for the H, L, and LL groups.

Meteorite group	n	Weighted average grain density (g/cm^3)	Average bulk density (g/cm^3)	Weighted average porosity (%)	Average porosity (%)	Porosity range (%)
H	15	3.67 ± 0.04	3.39	8.3 ± 1.0	6.9	0–27
L	21	3.39 ± 0.03	3.31	3.7 ± 1.0	1.7	0–14
LL	6	3.44 ± 0.05	3.28	8.0 ± 1.7	7.5	0–18

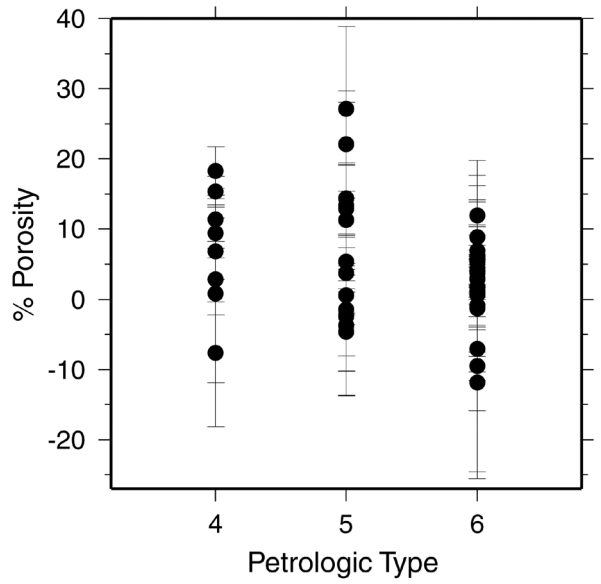


Fig. 4. Plot of percent porosity versus petrologic grade. Petrologic grade represents the amount of heating the ordinary chondrite has undergone. No correlation is evident between porosity and petrologic grade.

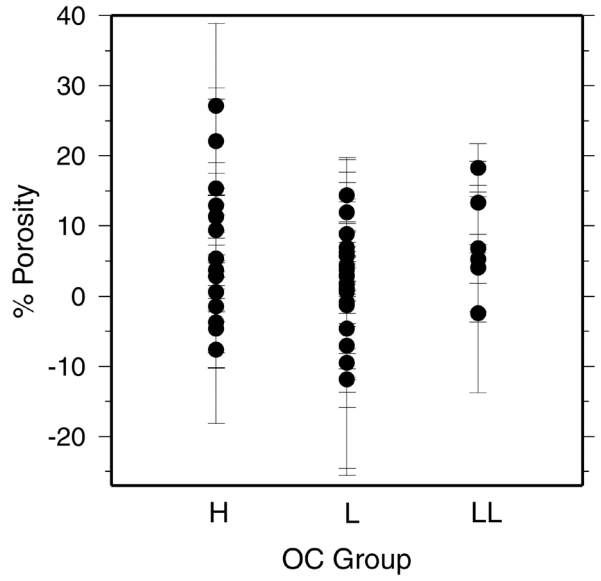


Fig. 5. Plot of percent porosity versus ordinary chondrite chemical group. Ordinary chondrites are divided into three chemical groups (LL, L, and H) based on total iron and total metal content. No correlation exists between porosity and chemical group.

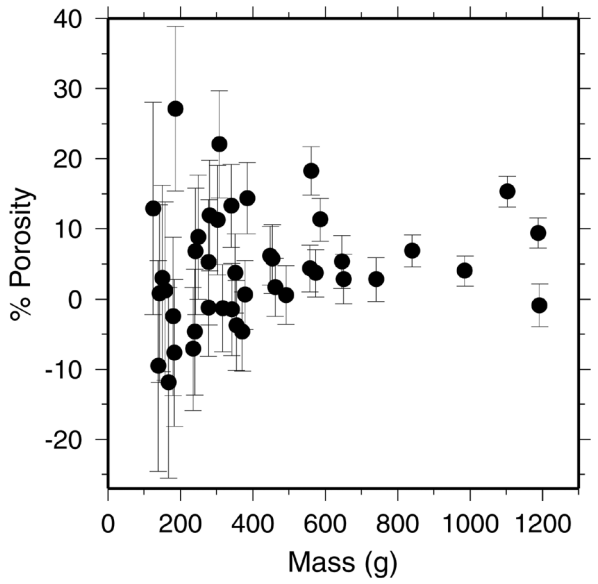


Fig. 6. Plot of percent porosity versus sample mass. Error bars are larger for small samples because smaller sized samples are more affected by the constant grain volume error. Note that porosities shown as negative are consistent with zero after taking into account the error in the measurement.

As a first-order effect, bulk elemental composition controls the density of a meteorite (i.e., types of meteorites such as irons and stones can be divided into categories based on density). However, a study of the bulk densities of 82 samples of 72 ordinary chondrite meteorites showed that bulk chemical composition is independent of bulk density within the ordinary chondrite group of meteorites (Wilkison and Robinson 2000). Wilkison and Robinson (2000) suggested that porosity was the predominant control of bulk density variations within the ordinary chondrites. Our data do not support this conclusion; porosity and bulk density are uncorrelated (Fig. 7a). Porosity and grain density may be weakly correlated (Fig. 7b), however, the errors due to the grain volume measurement limit the resolution of these data.

Twelve samples of 10 ordinary chondrites (see Table 1) measured for density and porosity in this study are classified as brecciated (cf., Grady 2000). We found no correlation between sample porosity and brecciated texture.

Studies that examined the relationship of impact shock on the porosity of rocks suggest that shock should decrease the pore spaces of the target rock. For example, shocked Coconino sandstone shows less porosity than massive unshocked Coconino sandstone (Kiefer 1971). The decrease in porosity

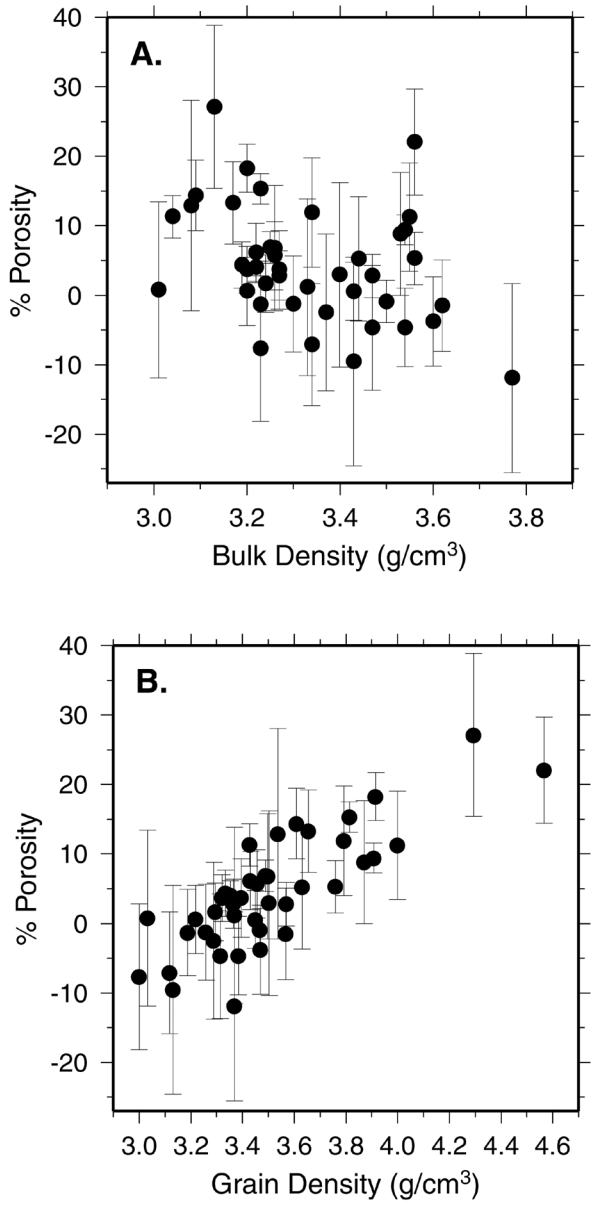


Fig. 7. Plots of percent porosity versus density: a) porosity and bulk density are uncorrelated (correlation coefficient [r] is 0.3); b) porosity and grain density may be weakly correlated, but due to the high experimental error in the grain volume determination, this is difficult to confirm with our data. The correlation coefficient (r) is 0.7.

occurred by translation and rotation of grains into the pores (for 3.5 GPa or less of pressure) or by the plastic flow of grains around each other and into pore spaces (for 3.5 to 13 GPa of pressure) (Kiefer 1971). An increase in porosity for rocks shocked to above 35 GPa of pressure is also reported, suggesting that the presence of vesicular glass increases the porosity (Kiefer 1971). Schall and Horz (1980) performed shock experiments on lunar soil, concluding that the initial pore space was collapsed in each sample. Samples shocked to less than 50 GPa had low porosities, but samples shocked to higher pressures (between 65 to 73 GPa) had higher porosities due to vesicles within shock melts (Schall and Horz 1980). In contrast, Kukkonen et al. (1992) reported an increase in porosity in impact melts, suevites, and impact breccias of the Lappajarvi crater compared to the surrounding crystalline basement rock; the study did not address the specific pressures to which the rocks had been shocked. To determine if any trend can be definitively shown in meteorite samples, we compared our porosity results to ordinary chondrite shock level.

Stöffler et al. (1991) developed a shock classification system for ordinary chondrite meteorites based on the identification of shock effects in olivine and plagioclase in thin sections. The meteorites measured for porosity in this study for which no previous shock classification existed were examined under thin section and classified (see Table 1) according to the effects defined by Stöffler et al. (1991). Our samples ranged from unshocked (S1, less than 4–5 GPa) to strongly shocked (S5, between 45–55 GPa). No samples measured in this study are classified as S6 (very strongly shocked, between 75–90 GPa). As is typical of ordinary chondrite meteorites (Stöffler et al. 1991), most of the samples are classified as S3 (weakly shocked, between 15–20 GPa). Within these shock levels, we find no correlation between shock stage and porosity (Fig. 8). However, we measured few samples classified as S4 or greater; to conclusively understand the relationship between shock and porosity, more samples at higher shock levels would need to be measured for porosity. Consolmagno et al. (1998) proposed an ordinary chondrite porosity model that predicts that less severely shocked ordinary chondrites should show a broad range of porosities, while more heavily shocked ordinary chondrites should show a smaller range of porosities. The porosity model proposes that heavily shocked meteorites rarely or never have large porosities (Consolmagno et al. 1998). Even though one would expect some relationship between shock and porosity, none was observed with our study.

Heterogeneity within Ordinary Chondrites

To investigate the range of heterogeneity in both porosity and density within a meteorite, we examined shower stones. The study of meteorites from a single shower minimizes the potential differences in chemical group or petrologic grade seen between stones from different falls. One would assume that stones from the same shower should be nearly identical in composition and other physical properties. However, some evidence exists for heterogeneity in both bulk density and porosity among shower stones (Wilkison and Robinson 2000; Consolmagno and Britt 1998). Wilkison and Robinson (2000) noted a significant variation in bulk density (3.31 to 3.63 g/cm^3) between 11 pieces of Pultusk. A study of the grain and bulk densities and porosities of four pieces of Pultusk suggests relative homogeneity in porosity but heterogeneity in bulk density (Consolmagno and Britt 1998). The bulk densities of these Pultusk pieces ranged from 3.38 to 3.51 g/cm^3, resulting

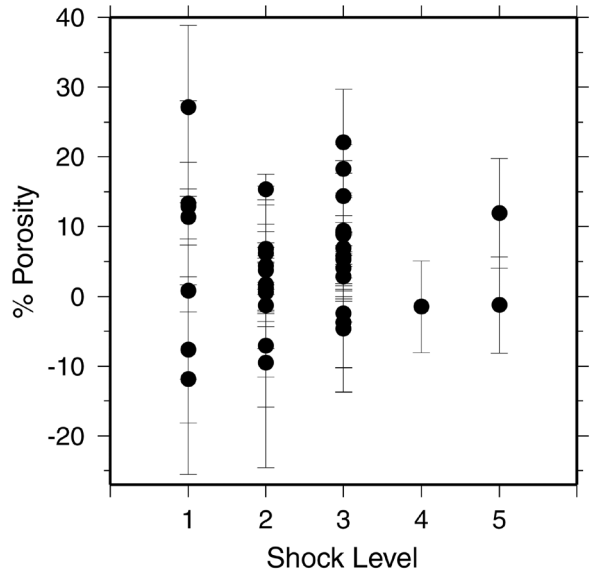


Fig. 8. No correlation between porosity and shock level (as defined in Stöffler et al. 1991) is observed; however, few samples with classifications of S4 or greater were measured.

in an average porosity between 3.0–6.4% (Consolmagno and Britt 1998). Consolmagno and Britt (1998) did not measure the four individual pieces of Pultusk for grain density but measured the average grain density (3.61 g/cm^3) by putting all the pieces within the pycnometer at one time. However, if a large variation in grain density between the pieces existed, then the porosities reported based on the average grain density may be different than the actual porosity. To avoid this ambiguity, we measured individual pieces for both grain and bulk density to determine porosity. We report the first data set on both porosity and density measured on individuals of a group of shower-forming stones.

To investigate the variations in bulk and grain density reported in Consolmagno and Britt (1998) and Wilkison and Robinson (2000), we hoped to measure the porosities of multiple pieces of Pultusk. Unfortunately, most of the pieces of Pultusk available for this study are not large enough to be measured reliably for grain density by our pycnometer. Thus, we were only able to measure three pieces of Pultusk, with porosities of –3.8% ± 6.4%, –4.6% ± 5.7%, and 5.3% ± 3.8% (the weighted average porosity of the pieces is 1.1% ± 2.8%). The grain densities of the pieces were 3.47 g/cm^3, 3.38 g/cm^3, and 3.76 g/cm^3. Even though the three pieces show variations in grain density, the differences between the values are consistent within the experimental error; the porosities of the three Pultusk stones are identical within the error. However, with only three samples, we cannot definitively conclude that porosity and density are homogeneous among all pieces of this fall.

Holbrook is an L6 ordinary chondrite that fell in 1912 near Holbrook, Arizona as a shower of stones ranging in sizes from 6.6 kg to less than 0.1 g (Foote 1912; Gibson 1970). A total of about 244 kg fell, mostly in small stones that are estimated to number over 16,000 (Gibson 1970). We examined nine pieces of Holbrook large enough to be reliably measured in our pycnometer. The weighted average of the porosity of the pieces was 2.7% ± 1.6%, ranging from 0% to 6.2%. The Holbrook stones exhibited bulk densities and porosities that varied slightly beyond the analytical uncertainties.

Variations in density between pieces of a single fall could be due to either variations in original chemical composition between the stones or to alteration in chemical composition caused by varying amounts of terrestrial weathering among several of the stones. Pieces of Holbrook have been shown to have undergone slight amounts of terrestrial weathering, depending on when the piece was picked up from the fall location (Gibson and Bogard 1978; Bland et al. 1998a). Terrestrial weathering has been shown to affect bulk elemental composition of ordinary chondrites (Gibson and Bogard 1978; Bland et al. 1998b) and has been suggested as a mechanism by which the porosity of a meteorite decreases. However, some workers have proposed that weathering products would block pores, reducing the ability of water to penetrate the meteorite, and, thus, slow further degradation and alteration (Bland et al. 1996; Gooding 1986). To further test which of these theories could be the cause of the slight density differences observed in Holbrook, one could measure weathering effects with ^{57}Fe Mössbauer spectroscopy and measure chemical variations with bulk elemental geochemistry on the specific samples of Holbrook measured for density and porosity in this study.

In summary, our examination of pieces of Pultusk and Holbrook suggest relative homogeneity in porosity and density between pieces from the same shower, although more measurements should be compiled to verify this conclusion. Only slight differences in bulk density and porosity exist among the pieces of Holbrook; any 200–600 g piece of Holbrook appears to be representative of the entire Holbrook mass. Our data on the three samples of Pultusk indicate homogeneity in bulk density, in contrast to the conclusions of Wilkison and Robinson (2000). We speculate that the significant variations in bulk density observed in Pultusk by Wilkison and Robinson (2000) could be due to variations in shock veining (Stöffler et al. 1991) between individual pieces of Pultusk or chemical inhomogeneity within the Pultusk meteorite. In addition, even though the grain and bulk densities of each fall are very different from each other (see Table 1), the porosities of Pultusk (~1%) and Holbrook (~3%) are similar to each other. The porosity values for both showers fall in the low end of the range of all ordinary chondrites (–12% to 27%) and are low relative to the average porosity of 6.4%.

Friable Ordinary Chondrites

Even though friable ordinary chondrites are often noted in the literature (e.g., Merrill and Stokes 1900), these

meteorites have garnered more attention recently given the low-density measurements of many asteroids. Some authors interpret the low density of some asteroids to indicate the presence of macroporosity (i.e., Consolmagno and Britt 1998; Wilkison and Robinson 2000; Wilkison et al. 2002; Britt et al. 2002), while others infer that the rare group of highly-friable, porous meteorites may be more representative of the original microporosity of their parent bodies (Flynn et al. 1999). To investigate if these ordinary chondrites could be meteorite analogues to low-density asteroids, we have undertaken a study of the densities and porosities of two particularly friable ordinary chondrites (Bjurböle and Allegan).

The L4 Bjurböle meteorite (330 kg total recovered) fell in Finland in 1899 and broke into fragments, the largest of which weighed 80 kg (Ramsay and Borgstrom 1902). The Smithsonian Institution holds specimens of Bjurböle ranging in mass from a few mg (e.g., individual chondrules) to more than 400 g. The 142 g piece of Bjurböle that we measured is not extremely friable (compared to samples at the Field Museum of Natural History and samples described in Flynn et al. [1999]), and its porosity is 0.8% ± 12.7% (as described above, the large error in porosity is due to the small sample size). The pieces of Bjurböle measured by Flynn et al. (1999) were described as being extremely crumbly and friable, and they determined the porosity of two pieces (29.31 g and 10.84 g) to be 20% and 23%, respectively. We emphasize that a substantial difference in porosity and friability exists between the pieces examined in this study and in Flynn et al. (1999).

Allegan is an H5 chondrite that fell as a single stone in Allegan County, Michigan on July 10, 1899; it shattered as it impacted the ground (Ward 1899; Merrill and Stokes 1900). Merrill and Stokes (1900) and Ward (1899) describe Allegan as being exceedingly friable (i.e., crumbling readily between the thumb and finger). Allegan is also an unweathered meteorite, free from oxidation products (Merrill and Stokes 1900; Mason and Maynes 1967; Bland et al. 1997). Previous studies have reported varying densities for Allegan samples. Merrill and Stokes (1900) measured the specific gravity of Allegan to be about 3.905 via a picnometer flask. Ward (1899) measured the specific gravity of a crustless piece of a 1.8 kg fragment to be 3.558. Mason and Maynes (1967) measured the grain density of a piece of Allegan to be 3.75 g/cm^3. We measured the densities and porosities of two fusion-crusted fragments of Allegan. One piece (FMNH Me 1432) has a porosity of 27%, a grain density of 4.29 ± 0.69 g/cm^3, and is more friable than the other piece measured (FMNH Me 1430), which has a porosity of 13% and a grain density of 3.54 ± 0.61 g/cm^3. Just as with Bjurböle, there are substantial differences in porosity and friability between the two pieces of Allegan.

Bjurböle and Allegan are complicated examples of a rare group of ordinary chondrites because they are equilibrated (and, thus, metamorphosed) yet retain friability and porosity compared to other ordinary chondrites. In addition, significant variability in both friability and porosity exists between pieces of the same fall. To account for this variability, we investigate two possible environments of formation for these meteorites.

First, perhaps the variations in friability and porosity are due to the individual pieces' original depth within a parent body that accreted with a high microporosity. This explanation seems less likely to explain Allegan, which fell as a single stone (~32 kg) that exhibits a range of porosity and friability. Because Allegan fell as a single piece, it probably represents a single location within its parent body. Also recall that Allegan was immediately curated after its fall, minimizing terrestrial alteration. A more likely explanation is that the porous parent body did not have uniform friability and porosity throughout, possibly due to physical inhomogeneities from the time of accretion or subsequent alteration during impact events. An example of an asteroid that may have accreted with a high microporosity is 253 Mathilde. The low bulk density estimate (1.3 ± 0.2 g/cm^3) and the existence of craters with diameters equal to or greater than Mathilde's radius suggests that the asteroid has an average porosity of ~50% (Yeomans et al. 1997; Veverka et al. 1997; Thomas et al. 1999; Cheng and Barnouin-Jha 1999). One theory proposed to explain this porous structure is that Mathilde originally accreted as a porous object (Yeomans et al. 1997; Veverka et al. 1997; Thomas et al. 1999; Cheng and Barnouin-Jha 1999). Because of the existence of a highly porous asteroid like Mathilde, we believe that other asteroids may share this characteristic porous structure. Mathilde, however, is a C-type asteroid and, thus, not a potential analogue to the friable ordinary chondrites of our study. Mineralogical and chemical evidence suggests that the S-class asteroid 433 Eros has a composition most similar to an ordinary chondritic composition (Trombka et al. 2000; Nittler et al. 2001; McFadden et al. 2001; McCoy et al. 2001; Evans et al. 2001). For the purpose of this discussion, we assume that S-type asteroids (such as 433 Eros and 243 Ida) are the parent bodies of ordinary chondrite meteorites. If Ida and Eros had formed with high microporosity, their bulk densities should match that of their ordinary chondrite analogues. The bulk densities of Ida (2.60 ± 0.5 g/cm^3) (Belton et al. 1995) and Eros (2.67 ± 0.03 g/cm^3) (Veverka et al. 2000; Yeomans et al. 2000) are at the low end of the range (2.64 to 3.13 g/cm^3) of bulk densities for friable, porous ordinary chondrites (from this study and Flynn et al. [1999]). However, surface structural evidence (Prockter et al. 2002; Cheng et al. 2002) suggests that Eros has significant fracturing and, thus, a significant amount of macroporosity. Ida also shows evidence of structural features such as grooves, which are proposed to represent reactivated fractures in the asteroid's interior (Sullivan et al. 1996). Therefore, the idea that Ida or Eros are examples of asteroids that accreted with a high microporosity is unlikely.

Second, the friable meteorites' physical properties could be due to secondary processes rather than being

representative of the density and porosity of the asteroid as a whole. These ordinary chondrites could be rocks that formed in the regolith or in a fault zone of the parent body, such as a regolith, fragmental, or fault breccia. A regolith breccia forms by impact lithification of unconsolidated material (cf., Keil 1982). An example of regolith materials indurated by impact is the friable regolith breccia sampled at Van Serg crater at the Apollo 17 site (Schmitt 1973). Regolith breccias typically exhibit evidence of being on the surface of a body, such as solar wind implantation, solar flare tracks, agglutinates, etc. (cf., Keil 1982). Fragmental breccias consist of rock and mineral fragments of differing lithologies (Bunch and Rajan 1988); they lack evidence of surface exposure but may have cogenetic material (Keil 1982). A fault (micro)breccia is formed by shearing along a fault. Evidence indicative of fault breccias includes clasts with morphologies associated with fault action such as angular clasts, clasts that show fractures and displacement, fault gouge, and angular clasts set in a matrix of small lithic fragments. Results from NEAR Shoemaker show that 433 Eros has a pervasive and complex regolith, typically tens of meters thick (Veverka et al. 2001; Robinson et al. 2002), that exhibits a gradation of consolidation states (Robinson et al. 2002). For example, boulders range from loosely aggregated to coherent and angular (Fig. 9). Studies of the large- and small-scale topography of Eros show evidence of scarps and other fractures (Cheng et al. 2002; Prockter et al. 2002; Thomas et al. 2002b), indicating a coherent substrate. The regolith and/or the deep fractures seen on the surface of Eros are ideal locations to find low density/high porosity material to form potentially friable meteorites.

Neither Allegan nor Bjurböle are specifically classified as a breccia. However, both meteorites have some evidence indicating that they could have formed as impact rocks. Scott et al. (1985) identified three anomalous clasts within Bjurböle that could not have been metamorphosed in situ (indicating that Bjurböle is a breccia). Scott et al. (1985) propose that Bjurböle and other chondrites with anomalous clasts are a type of fragmental breccia in which the anomalous clasts are mixed with host material after the peak metamorphic temperatures experienced by the host material have been reached. McCoy (1990) reported evidence from the compositions of chondrule silicates, ranges of metallographic cooling rates, and variations in matrix rim textures that chondrules from ALH A77278 (LL 3.0–4) and Hamlet (LL 3.9) experienced diverse thermal histories prior to incorporation into the meteorites. We speculate that both Allegan and Bjurböle may be fragmental breccias formed within the regolith of their parent bodies. Further analysis of the bulk geochemistry and petrology of porous, friable ordinary chondrites for evidence of anomalous clasts, of surface exposure, or that their chondrules have experienced diverse thermal histories would be required to validate if the meteorites could be classified as breccias.

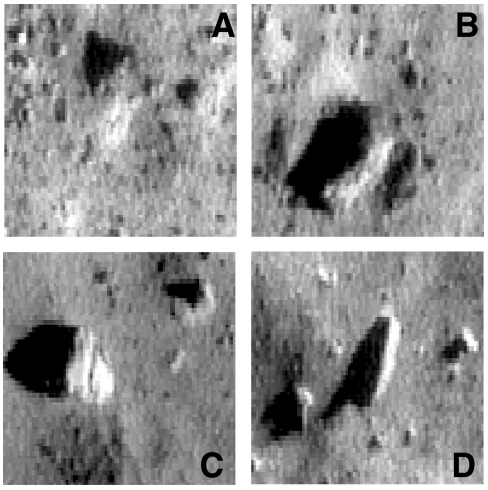


Fig. 9. A range of consolidation states (a–d) exists among boulders on the surface of Eros, from completely degraded and disintegrating boulders to angular and coherent boulders (Thomas et al. 2002b; Robinson et al. 2002). The complex regolith of Eros could be an ideal location to find low density/high porosity material to form potentially friable meteorites: a) extremely degraded boulder on the surface of asteroid 433 Eros. Image 155907726 at 36.0° S, 342.7° W. The boulder size is about 73 m; b) degraded boulder. Image 155815311 at 16.7° S, 352.7° W. The boulder size is about 128 m; c) angular and cleaved boulder. Image 156082716 at 8.7° S, 1.7° W. The boulder diameter is about 27 m; d) angular boulder. Image 156077251 at 8.7° S, 198.0° W. The diameter of the boulder is about 63 m.

Asteroid Porosity Estimates

Using an average microporosity of 6%, an average bulk density of ordinary chondrites (3.40 g/cm^3) and the bulk density determination of 433 Eros derived from NEAR data (2.67 ± 0.03 g/cm^3) (Veverka et al. 2000; Yeomans et al. 2000), Wilkison et al. (2002) estimated that Eros could have 20% macroporosity. The average microporosity (6%) and the overall range of ordinary chondrite porosities (0–15%) used in Wilkison et al. (2002) was based on ~40 ordinary chondrite porosity measurements (Consolmagno and Britt 1998; Flynn et al. 1999). With the addition of these 42 new measurements, the range of porosities and the average ordinary chondrite porosity is better constrained. The weighted average of our 42 porosity measurements is 6.4%, similar to that of the previous studies (6%) (Consolmagno and Britt 1998; Flynn et al. 1999). The total range of our ordinary chondrite porosities is −12 to 27%. Using the weighted average of 6.4% porosity, we estimate an average macroporosity of about 20% for Eros (consistent with Wilkison et al. [2002]).

The densities and porosities of several samples of other types of meteorites (Table 3) were also measured. These additional measurements are useful to determine more about the porosities of different classes of asteroids and give further clues as to potential asteroidal internal structure. For example, a future mission such as the DAWN Discovery

Table 3. Densities and porosities of other types of meteorites measured in this study.

Meteorite name	Sample no.	Type	Mass	Grain volume (cm^3)	Grain density (g/cm^3)	Bulk volume (cm^3)	Bulk density (g/cm^3)	Porosity (%)
Allende	FMNH ME 2636	CV3.2	328.79	96.2 ± 8.6	3.42 ± 0.31	110.3 ± 1.3	2.98 ± 0.04	12.8 ± 7.9
Murchison	FMNH ME 2752 24a	CM2	310.01	114.8 ± 5.7	2.70 ± 0.13	127.6 ± 1.7	2.43 ± 0.03	10.0 ± 4.6
	FMNH ME 2752 24b	CM2	353.00	130.2 ± 5.7	2.71 ± 0.11	150.9 ± 1.6	2.34 ± 0.03	13.7 ± 3.4
Crab Orchard	FMNH ME 1262	MES	814.20	190.0 ± 5.8	4.28 ± 0.13	201.5 ± 3.6	4.04 ± 0.07	5.7 ± 3.3
	FMNH ME 185	MES	477.39	91.2 ± 5.4	5.24 ± 0.31	112.3 ± 1.4	4.25 ± 0.05	18.8 ± 4.9
Estherville	FMNH ME 1305	MES	227.13	38.1 ± 6.8	5.96 ± 1.07	49.6 ± 0.7	4.58 ± 0.06	23.1 ± 13.8
Imilac	FMNH ME 742	PAL	392.00	86.4 ± 5.8	4.54 ± 0.30	–	–	–
Cumberland Falls	FMNH ME 1996	AUB	879.50	279.9 ± 5.5	3.14 ± 0.06	279.2 ± 3.9	3.15 ± 0.04	–0.3 ± 2.4
Ibitira	NMNH 6860	EUC	317.30	107.4 ± 5.7	2.96 ± 0.16	–	–	–
Hvittis	FMNH ME 1470	E6	367.44	101.4 ± 6.3	3.62 ± 0.23	100.9 ± 1.2	3.64 ± 0.04	–0.5 ± 6.3

Mission plans to investigate the asteroids 1 Ceres and 4 Vesta. Achondrites represent "crustal" layers from a differentiated body, thus, the densities of meteorites like Cumberland Falls are useful in predicting a density distribution for a differentiated body such as Vesta (Thomas et al. 1997; Keil 2002).

CONCLUSIONS

We measured the densities and porosities of 42 samples of 30 ordinary chondrite meteorites. The porosities of these samples range from −12 (essentially zero) to 27%. The weighted average porosity of the 42 samples is 6.4%. We also performed a rigorous quantification of the errors associated with the grain volume measurement method, and determined that the helium gas pycnometer used in this study can determine the grain volume of a sample to ~±6 cm^3. Potential controls of ordinary chondrite porosity were investigated; based on these new measurements, we conclude that no correlation exists between porosity and petrologic grade, chemical group, mass, density, or shock level among ordinary chondrite meteorites. We investigated the range of heterogeneity in porosity and density among stones from a single shower. Even though a limited number of stones from both Pultusk and Holbrook were measured, there appears to be relative homogeneity among the stones from these falls. Finally, we examined two friable and porous ordinary chondrites, Allegan and Bjurböle, to consider if these meteorites can be analogues for low-density asteroids. We conclude that these meteorites may be secondary products (breccias) that formed within the regolith or fault zones of S-type asteroids.

Acknowledgments–The authors would like to thank the following for their contributions with technical and/or sample assistance: Paul Delacoe (Core Laboratories), Craig Whitney (Core Laboratories), and Bill Remien (Northwestern University). We thank Meenakshi Wadhwa and Clarita Nuñez for the loan of the specimens from the Field Museum of Natural History. A special thanks goes to G. J. Consolmagno S. J., for valuable discussions regarding data reduction. We thank G. Consolmagno, A. Brearley, and I. Lyon for helpful reviews of the manuscript.

Editorial Handling—Dr. Ian Lyon

REFERENCES

Belton M. J. S., Chapman C. R., Thomas P. C., Davies M. E., Greenberg R., Klassen K., Byrnes D., D'Amario L., Synnott S., Johnson T. V., McEwen A., Merline M. J., Davis D. R., Petit J. M., Storrs A., Veverka J., and Zellner B. 1995. Bulk density of asteroid 243 Ida from the orbit of its satellite Dactyl. *Nature* 374: 785–788.

Bennett M. E. and McSween H. Y. 1996. Shock features in iron-nickel metal and troilite of L-group ordinary chondrites. *Meteoritics & Planetary Science* 31:255–264.

Bland P. A., Berry F. J., Smith T. B., Skinner S. J., and Pillinger C. T. 1996. The flux of meteorites to the Earth and weathering in hot desert ordinary chondrite finds. *Geochimica et Cosmochimica Acta* 60:2053–2059.

Bland P. A., Kelley S. P., Berry F. J., Cadogan J. M., and Pillinger C. T. 1997. Artificial weathering of the ordinary chondrite Allegan; Implications for the presence of Cl- as a structural component in akaganeite. *American Mineralogist* 82:1187–1197.

Bland P. A., Berry F. J., and Pillinger C. T. 1998a. Rapid weathering in Holbrook: An iron-57 Mössbauer spectroscopy study. *Meteoritics & Planetary Science* 33:127–129.

Bland P. A., Sexton A. S., Jull A. J. T., Bevan A. W. R., Berry F. J., Thornley D. M., Astin T. R., Britt D. T., and Pillinger C. T. 1998b. Climate and rock weathering: A study of terrestrial age dated ordinary chondritic meteorites from hot desert regions. *Geochimica et Cosmochimica Acta* 62:3169–3184.

Britt D. T., Yeomans D., Housen K., and Consolmagno G. J. 2002. Asteroid density, porosity, and structure. In *Asteroids III,* edited by Bottke W., Cellino A., Paolicchi P., and Binzel R. P. Tucson: University of Arizona Press. pp. 485–500.

Britt D. T. and Consolmagno G. J. 2003. Stony meteorite porosities and densities: A review of the data through 2001. *Meteoritics & Planetary Science* 38:1161–1180.

Bunch T. E. and Rajan R. S. 1988. Meteoritic regolithic breccias. In *Meteorites and the early solar system,* edited by Kerridge J. K. and Matthews M. S. Tucson: University of Arizona Press. pp. 144–164.

Cheng A. F. and Barnouin-Jha O. 1999. Giant craters on Mathilde. *Icarus* 140:34–48.

Cheng A. F., Barnouin-Jha O., Prockter L. M., Zuber M. T., Neumann G., Smith D. E., Garvin J., Robinson M. S., Veverka J., and Thomas P. C. 2002. Small-scale topography of 433 Eros from laser altimetry and imaging. *Icarus* 155:51–74.

Consolmagno G. J. and Britt D. T. 1998. The density and porosity of meteorites from the Vatican collection. *Meteoritics & Planetary Science* 33:1231–1241.

Consolmagno G. J., Britt D. T., and Stoll C. P. 1998. The porosities of ordinary chondrites: Models and interpretations. *Meteoritics & Planetary Science* 33:1221–1229.

Evans L. G., Starr R. D., Bruckner J., Reedy R. C., Boynton W. V., Trombka J. I., Goldstein J. O., Masarik J., Nittler L. R., and McCoy T. J. 2001. Elemental composition from gamma-ray spectroscopy of the NEAR-Shoemaker landing site on 433 Eros. *Meteoritics & Planetary Science* 36:1639–1660.

Flynn G. J., Moore L. B., and Klock W. 1999. Density and porosity of stone meteorites: Implications for the density, porosity, cratering, and collisional disruption of asteroids. *Icarus* 142:97–105.

Foote W. M. 1912. Shower of meteorite stones, Arizona. *American Journal of Science* 34:437–456.

Geddis A. M. 1994. Rapid estimate of solid volume in large tuff cores using a gas pycnometer. M.S. thesis, University of Arizona. Tucson, Arizona, USA.

Gibson E. K. 1970. Discovery of another meteorite specimen from the 1912 Holbrook, Arizona fall site. *Meteoritics* 5:57–60.

Gibson E. K. and Bogard D. D. 1978. Chemical alterations of the Holbrook chondrite resulting from terrestrial weathering. *Meteoritics* 13:277–289.

Gomes C. B. and Keil K. 1980. *Brazilian stone meteorites.* Albuquerque: University of New Mexico Press. 162 p.

Gooding J. L. 1986. Clay-mineraloid weathering products in Antarctic meteorites. *Geochimica et Cosmochimica Acta* 50: 2215–2223.

Grady M. M. 2000. *Catalogue of Meteorites,* Fifth edition. Cambridge: Cambridge University Press. 689 p.

Grimm R. E. 1985. Penecontemporaneous metamorphism, fragmentation, and reassembly of ordinary chondrite parent bodies. *Journal of Geophysical Research* 90:2022–2028.

Herndon J. M. and Herndon M. A. 1977. Aluminum-26 as a planetoid heat source in the early solar system. *Meteoritics* 12:459–465.

Keil K. 1982. Composition and origin of chondritic breccias. In *Workshop on lunar breccias and soils and their meteoritic analogs,* edited by Taylor G. J. and Wilkening L. L. LPI Technical Report 82–02. Houston: Lunar and Planetary Institute. p. 65–83.

Keil K. 2002. Geological history of asteroid 4 Vesta: The "smallest terrestrial planet." In *Asteroids III,* edited by Bottke W. F., Cellino A., Paolicchi P., and Binzel R. P. Tucson: University of Arizona Press. pp. 573–584.

Kiefer S. W. 1971. Shock metamorphism of the Coconino Sandstone at Meteor Crater, Arizona. *Journal of Geophysical Research* 76: 5449–5473.

Kukkonen I. T., Kivekas L., and M. Paananen M. 1992. Physical properties of karnaite (impact melt), suevite, and impact breccia in the Lappajarvi meteorite crater, Finland. *Tectonophysics* 216: 111–122.

Mason B. and Maynes A. D. 1967. The composition of the Allegan, Bur-Gheluai, and Cynthiana meteorites. *Proceedings of the United States National Museum* 124:3624.

McCoy T. J. 1990. Metamorphism, brecciation, and parent body structures of LL-group chondrites. M.S. thesis, University of New Mexico, Albuquerque, New Mexico, USA.

McCoy T. J., Scott E. R. D., and Keil K. 1990. Metallographic cooling rates correlated with petrologic type in LL3.0–4 chondrites: Implications for parent body structures (abstract). 21st Lunar and Planetary Science Conference. pp. 749–750.

McCoy T. J., Burbine T. H., McFadden L. A., Starr R. D., Gaffey M. J., Nittler L. R., Evans L. G., Izenberg N., Lucey P., Trombka J. I., Bell J. F., Clark B. E., Clark P. E., Squyres S. W., Chapman C. R., Boynton W. V., and Veverka J. 2001. The composition of 433 Eros: A mineralogical-chemical analysis. *Meteoritics & Planetary Science* 36:1661–1672.

McFadden L. A., Wellnitz D. D., Schnaubelt M., Gaffey M. J., Bell J. F., Izenberg N., Murchie S., and Chapman C. R. 2001. Mineralogical interpretation of reflectance spectra of Eros from NEAR near-infrared spectrometer low phase flyby. *Meteoritics & Planetary Science* 36:1711–1726.

Merrill G. P. and Stokes H. N. 1900. A new stony meteorite from Allegan, Michigan, and a new iron from Mart, Texas. *Journal of the Washington Academy of Sciences* 2:41–68.

Millis R. L. and Dunham D. W. 1989. Precise measurement of asteroid sizes and shapes from occultations. In *Asteroids II,* edited by Binzel R. P., Gehrels T., and Matthews M. S. Tucson: University of Arizona Press. pp. 148–170.

Minster J. F. and Allegre C. 1979. ^{87}Rb-^{87}Sr chronology of H chondrites: Constraint and speculations on the early evolution of their parent body. *Earth and Planetary Science Letters* 42:333–347.

Miyamoto M. and Fujii N. 1980. A model of the ordinary chondrite parent body: An external heating model. *Memoirs of the National Institute of Polar Research* 17:291–298.

Miyamoto M., Fujii N., and Takeda H. 1981. Ordinary chondrite parent body: An internal heating model. Proceedings, 12th Lunar and Planetary Science Conference. pp. 1145–1152.

Nittler L. R., Starr R. D., Lim L., McCoy T. J., Burbine T. H., Reedy R. C., Trombka J. I., Gorenstein P., Squyres S. W., Boynton W, V., McClanahan T. P., Bhangoo J. S., Clark P. E., Murphy M. E., and Killen R. 2001. X-ray fluorescence measurements of the surface elemental composition of asteroid 433 Eros. *Meteoritics & Planetary Science* 36:1673–1695.

Pellas P. and Storzer D. 1981. ^{244}Pu fission track thermometry and its application to stony meteorites. *Proceedings of the Royal Society of London A* 374:253–270.

Prockter L. M., Thomas P. C., Robinson M. S., Joseph J., Milne A., Bussey B., Veverka J., and Cheng A. F. 2002. Surface expressions of structural features on Eros. *Icarus* 155:75–93.

Ramsay W. and Borgstrom L. H. 1902. Der Meteorit von Bjurböle bei Borgå. *Bulletin de la Commission Géologique de Finlande* 12:1–28.

Robinson M. S., Thomas P. C., Veverka J., Murchie S. L., and Wilcox B. B. 2002. The geology of 433 Eros. *Meteoritics & Planetary Science* 37:1651–1684.

Rubin A. E. 1992. A shock-metamorphic model for silicate darkening and compositionally variable plagioclase in CK and ordinary chondrites. *Geochimica et Cosmochimica Acta* 56: 1705–1714.

Rubin A. E. 1994. Metallic copper in ordinary chondrites. *Meteoritics* 29:93–98.

Schall R. B. and Horz F. 1980. Experimental shock metamorphism of lunar soil. Proceedings, 11th Lunar and Planetary Science Conference. pp. 1679–1695.

Schmitt H. H. 1973. Apollo 17 report on the valley of Taurus-Littrow. *Science* 182:681–690.

Scott E. R. D., Lusby D., and Keil K. 1985. Ubiquitous brecciation after metamorphism in equilibrated ordinary chondrites. *Journal of Geophysical Research* 90:137–148.

Scott E. R. D. and Rajan R. S. 1981. Metallic minerals, thermal histories, and parent bodies of some xenolithic, ordinary chondrites. *Geochimica et Cosmochimica Acta* 45:53–67.

Stöffler D., Keil K., and Scott E. R. D. 1991. Shock metamorphism of ordinary chondrites. *Geochimica et Cosmochimica Acta* 55: 3845–3867.

Sullivan R., Greeley R., Pappalardo R., Asphaug E., Moore J. M., Morrison D., Belton M. J. S., Carr M., Chapman C. R., Geissler P., Greenberg R., Granahan J., Head J. W., III, Kirk R., McEwen A., Lee P., Thomas P. C., and Veverka J. 1996. Geology of 243 Ida. *Icarus* 120:119–139.

Taylor G. J., Scott E. R. D., Rubin A. E., Maggiore P., and Keil K. 1982. Structure and fragmentation of the parent asteroids of ordinary chondrites (abstract). 13th Lunar and Planetary Science Conference. pp. 799–800.

Tedesco E. F., Veeder G. J., Fowler J. W., and Chillemi J. R. 1992. The IRAS Minor Planet Study. Phillips Laboratory Report PL-TR-92-2049.

Thomas P. C., Binzel R. P., Gaffey M. J., Storrs A. D., Wells E. N., and Zellner B. H. 1997. Impact excavation on asteroid 4 Vesta: Hubble Space Telescope results. *Science* 277:1492–1495.

Thomas P., Veverka J., Bell J. F., III, Clark B. E., Carcich B., and Joseph J. 1999. Mathilde: Size, shape, and geology. *Icarus* 140: 17–27.

Thomas P. C., Joseph J., Carcich B., Veverka J., Clark B. E., Bell J. F., Byrd A. W., Chomko R., Robinson M. S., Murchie S., Prockter L., Cheng A., Izenburg N., Malin M., Chapman C., McFadden L. A., Kirk R., Gaffey M., and Lucey P. G. 2002a. Eros: Shape, topography, and slope processes. *Icarus* 155:18–37.

Thomas P. C., Prockter L., Robinson M., Joseph J., and Veverka J. 2002b. Global structure of asteroid 433 Eros. *Geophysical Research Letters* 29:46-1–46-4.

Trombka J., Squyres S., Bruckner J., Boynton W., Reedy R., McCoy T., Gorenstein P., Evans L., Arnold J., Starr R., Nittler L., Murphy M., Mikheeva I., McNutt R., McClanahan T., McCartney E., Goldstein J., Gold R., Floyd S., Clark P., Burbine T., Bhangoo J., Bailey S., and Petaev M. 2000. The elemental composition of asteroid 433 Eros: Results of the NEAR-Shoemaker X-ray spectrometer. *Science* 289:2101–2105.

Veverka J., Thomas P., Harch A., Clark B., Bell J. F., III, Carcich B., Joseph J., Chapman C., Merline W., Robinson M., Malin M., McFadden L. A., Murchie S., Hawkins S. E., III, Farquhar R., Izenberg N., and Cheng A. 1997. NEAR's flyby of 253 Mathilde: Images of a C asteroid. *Science* 278:2109–2114.

Veverka J., Robinson M., Thomas P., Murchie S., Bell J., Izenberg N., Chapman C., Harch A., Bell M., Carcich B., Cheng A., Clark B., Domingue D., Dunham D., Farquhar R., Gaffey M., Hawkins E., Joseph J., Kirk R., Li H., Lucey M., Malin M., Martin P., McFadden L., Merline W., Miller J., Owen M., Peterson C., Prockter L., Warren J., Wellnitz D., Williams B., and Yeomans D. 2000. NEAR at Eros: Imaging and spectral results. *Science* 289: 2088–2097.

Veverka J., Thomas P., Robinson M., Murchie S., Chapman C., Bell M., Harch A., Merline W., Bell J., Bussey B., Carcich B., Cheng A., Clark B., Domingue D., Dunham D., Farquhar R., Gaffey M., Hawkins E., Izenberg N., Joseph J., Kirk R., Li H., Lucey P., Malin M., McFadden L., Miller J., Owen W., Peterson C., Prockter L., Warren J., Wellnitz D., Williams B., and Yeomans D. 2001. Imaging of small-scale features on 433 Eros from NEAR: Evidence for a complex regolith. *Science* 292:484–488.

Ward H. L. 1899. Notice of an aerolite that recently fell at Allegan, Michigan. *American Journal of Science* 8:412–414.

Wilkison S. L. and Robinson M. S. 2000. Bulk density of ordinary chondrite meteorites and implications for asteroidal internal structure. *Meteoritics & Planetary Science* 35:1203–1213.

Wilkison S. L., Robinson M. S., Thomas P. C., Veverka J., McCoy T. J., Murchie S. L., Prockter L. M., and Yeomans D. K. 2002. An estimate of Eros's porosity and implications for internal structure. *Icarus* 155:94–103.

Yeomans D., Barriot J. P., Dunham D. W., Farquhar R. W., Giorgini J. D., Helfrich C. E., Konopliv A. S., McAdams J. V., Miller J. K., Owen W. M. Jr., Scheeres D. J., Synnott S. P., and Williams B. G. 1997. Estimating the mass of asteroid 253 Mathilde from tracking data during the NEAR flyby. *Science* 278:2106–2109.

Yeomans D., Antreasian P., Barriot J., Chesley S., Dunham D., Farquhar R., Giorgini J., Helfrich C., Konopliv A., McAdams J., Miller J., Owen W., Scheeres D., Thomas P., Veverka J., and Williams B. 2000. Radio science results during the NEAR-Shoemaker spacecraft rendezvous with Eros. *Science* 289:2085–2088.

Yomogida K. and Matsui T. 1983. Physical properties of ordinary chondrites. *Journal of Geophysical Research* 88:9513–9533.

Zuber M. T., Smith D. E., Cheng A. F., Garvin J. B., Aharonson O., Cole T. D., Dunn P. J., Guo Y., Lemoine F. G., Neumann G. A., Rowlands D. D., and Torrence M. H. 2000. The shape of 433 Eros from the NEAR-Shoemaker Laser Rangefinder. *Science* 289: 2097–2101.